BIOCHEMISTRY
including biophysical chemistry & molecular biology

Article

pubs.acs.org/biochemistry

Molecular Dynamics Simulations of Barley and Maize Lipid Transfer Proteins Show Different Ligand Binding Preferences in Agreement with Experimental Data

Lorna J. Smith,*[,†] Ysobel Roby,[†] Jane R. Allison,[‡,§] and Wilfred F. van Gunsteren[‡]

[†]Department of Chemistry, University of Oxford, Inorganic Chemistry Laboratory, South Parks Road, Oxford OX1 3QR, United Kingdom

[‡]Laboratory of Physical Chemistry, Swiss Federal Institute of Technology ETH, Wolfgang-Pauli-Strasse 10, 8093 Zürich, Switzerland

Supporting Information

ABSTRACT: Experimental studies of barley and maize lipid transfer proteins (LTPs) show that the two proteins bind the ligand palmitate in opposite orientations in their internal cavities. Moreover, maize LTP is reported to bind the ligand caprate in the internal cavity in a mixture of two orientations with approximately equal occupancy. Six 30 ns molecular dynamics (MD) simulations of maize and barley LTP with ligands bound in two orientations (modes M and B) have been used to understand the different ligand binding preferences. The simulations show that both maize and barley LTP could bind palmitate in the orientation observed experimentally for maize LTP (mode M), with the predominant interaction being a salt bridge between the ligand carboxylate headgroup and a conserved arginine side chain. However, the simulation of barley LTP with palmitate in the mode B orientation shows the most favorable protein−ligand interaction energy. In contrast, the simulations of maize LTP with palmitate and with caprate in the mode B orientation show no persistent ligand binding, the ligands leaving the cavity during the simulations. Sequence differences between maize and barley LTP in the AB loop region, in residues at the base of the hydrophobic cavity, and in the helix A region are identified as contributing to the different behavior. The simulations reproduce well the experimentally observed binding preferences for palmitate and suggest that the experimental data for maize LTP with caprate reflect ligand mobility in binding mode M rather than the population of binding modes M and B.

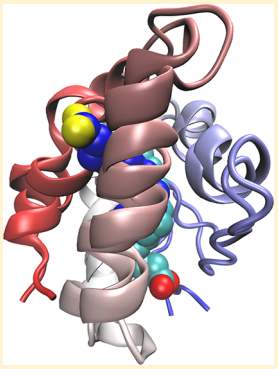

Plant nonspecific lipid transfer proteins 1 (LTPs) make up an important class of proteins that contain an internal cavity in which a broad range of lipid and related molecules can bind, including phospholipids, glycolipids, acyl-coenzyme A, fatty acids, hydroxylated fatty acids, and prostaglandins.[1−3] The role of plant LTPs *in vivo* is not completely understood, but it is recognized that they are involved in plant defense against bacterial and fungal pathogens and probably also in cuticular wax formation and plant growth and development.[4−7] These proteins are also significant because of their involvement in IgE-mediated food allergies.[3]

Plant LTPs are found in a wide range of species, including cereals, fruits, vegetables, and nuts.[1,6] The proteins share a high degree of sequence similarity and a common structural fold.[1,2,8] They consist of four α-helices, held together by a network of four conserved disulfide bridges, and an extended C-terminal region with no regular secondary structure.[2,3] The internal cavity in which the ligands bind is found within the helical core of the protein, and the C-terminal region acts as a lid over the bottom of the cavity. A number of structures of plant LTPs bound to a variety of ligands have been determined.[9−17] An interesting and curious finding from these experimental structure determinations is that, despite the conserved sequence and fold of the proteins, not all LTPs bind the same ligand in the same orientation.[7] In particular, barley LTP binds the ligand palmitate in a manner inverted compared to that of maize LTP.[9,11] In addition, maize LTP is reported to bind the ligand caprate in the internal cavity in a mixture of the two orientations with approximately equal occupancy.[13] Furthermore, in the structure of rice LTP with palmitate, two ligand molecules are bound simultaneously in the cavity, in a head-to-tail manner with opposite orientations.[15] Dual ligand binding in the internal cavity is also seen in the structure of wheat LTP with lyso-myristoyl-phosphatidylcholine.[14]

Structural genomics analyses have identified a wide range of subtle sequence differences between homologous proteins in different species and also possibilities for many point mutations within a given protein sequence. Many of these sequence changes have little effect on the structure or function of the protein concerned, although sometimes changes in just one residue can have a profound effect.[18−22] Maize LTP and barley LTP are 55% identical and 72% similar in sequence [using the Needleman−Wunsch alignment algorithm[23] (Figure 1)]. The identical residues include many of those that line the internal cavity where the ligands bind. Both proteins show the

Received: May 24, 2013
Revised: July 8, 2013
Published: July 8, 2013

   dx.doi.org/10.1021/bi4006573 | *Biochemistry* 2013, 52, 5029−5038

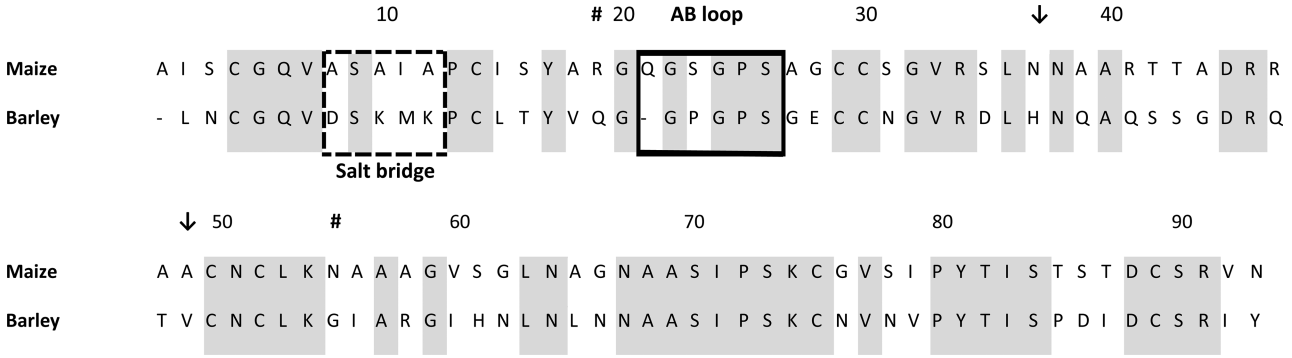

Figure 1. Alignment of the sequences of maize and barley LTP. The alignment was made with the EMBOSS (European Molecular Biology Open Source Software Suite) needle utility,[42] which uses the Needleman–Wunsch alignment algorithm[23] for the alignment of two sequences. The conserved residues are shaded, and the residue numbering given is that for maize LTP. The positions of sequence differences between mLTP and bLTP discussed in the text are indicated in the following manner: the AB loop region is shown in a solid box, and the part of helix A where there is a persistent salt bridge between the side chains of Asp 7 and Lys 11 in bLTP is shown in a dashed box. Sequence differences for residues in the LTP internal cavity are shown by downward-pointing arrows, and changes at the entrance to the cavity in binding mode B are indicated with a number sign.

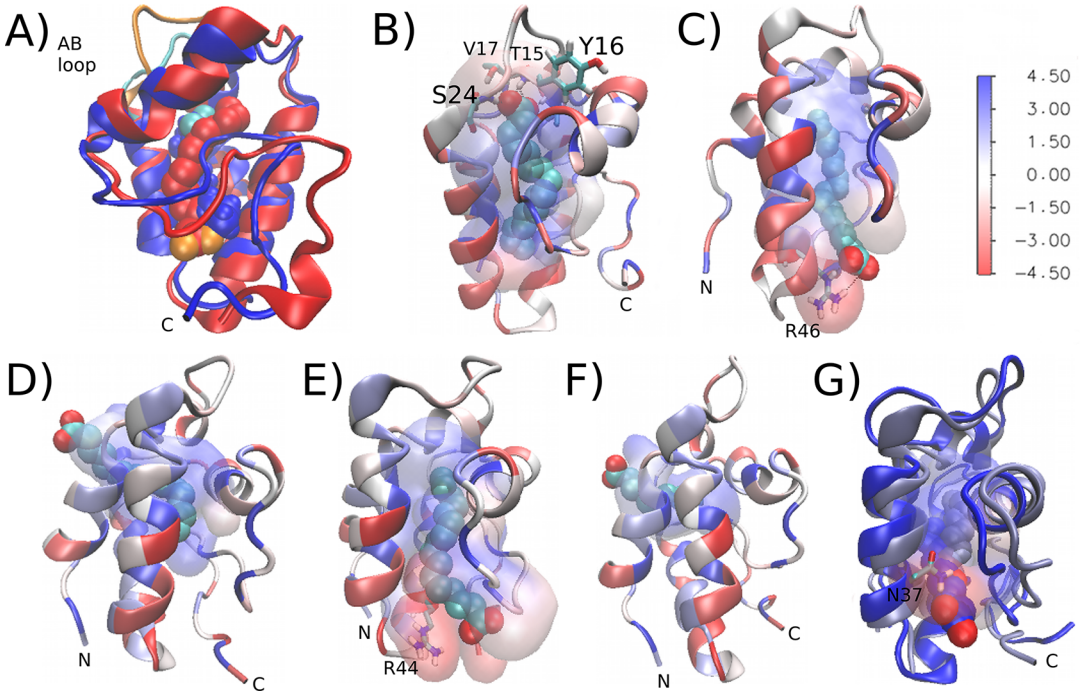

Figure 2. Illustrations of palmitate and caprate binding to bLTP and mLTP. (A) Overlay of (blue) the bLTP–palmitate NMR model structure (PDB entry 1be2, model 1) and (red) the mLTP–palmitate X-ray structure (PDB entry 1mzm) showing that they have similar structures but different ligand binding modes. The carbonyl oxygens of the palmitate ligand and the AB loop regions are colored cyan (bLTP) and orange (mLTP). The C-terminus is labeled; the N-terminus is at the back in this view. (B–E) Positions of palmitate at the end of the (B) bLTP_PLM_B, (C) bLTP_PLM_M, (D) mLTP_PLM_B, and (E) mLTP_PLM_M simulations. The protein structures (cartoon) and binding surfaces experienced by the ligand (surface) are colored according to the Kyte–Doolittle hydrophobicity scale (per residue) as indicated with the color scale, where more negative numbers indicate more hydrophilic residues and vice versa. The palmitate atoms are colored according to type: cyan for carbon and red for oxygen. Residues that form hydrogen bonds or salt bridges with the ligand are shown where relevant: (B) Thr 15, Tyr 16, Val 17, and Ser 24; (C) Arg 46; and (E) Arg 44. (F and G) Positions of caprate at the end and (G only) during the (F) mLTP_CPR_B and mLTP_CPR_M simulations. In panel F, the coloring is the same as that in panels B–E. In panel G, the structures of mLPT and caprate after simulation for 20 ns are colored pale blue and at the end of the simulation (after 40 ns) dark blue. The binding surface is colored according to hydrophobicity, and the oxygen atoms and Asn 37 are colored according to type as in panels B–E. This figure was generated using VMD.[29]

nonspecific ligand binding characteristics of LTPs and will bind a range of lipid-like molecules in their internal cavities. However, as identified above, the binding mode for the ligand palmitate is inverted in barley LTP (bLTP) compared to that in maize LTP (mLTP). These proteins therefore provide an ideal opportunity to consider how small changes in protein residue sequence can radically alter ligand binding behavior in a mainly hydrophobic internal cavity. To explore this issue, we have used molecular dynamics simulations of mLTP–palmitate, mLTP–caprate, and bLTP–palmitate complexes. In each case, simulations have been performed with the ligand bound in two orientations, M and B (Figure 2A). Mode M is seen in the

dx.doi.org/10.1021/bi4006573 | *Biochemistry* 2013, 52, 5029–5038

Table 1. Summary of the Simulations of Maize and Barley LTP[a]

simulation name	sequence	ligand	binding mode	starting structure	no. of water molecules	no. of Cl^- ions
bLTP_PLM_B	barley	palmitate	B	1be2	8442/8251	2/1
bLTP_PLM_M	barley	palmitate	M	1be2 with ligand inverted	8442/8251	2/1
mLTP_PLM_B	maize	palmitate	B	1mzm with ligand inverted	8006/8494	6/5
mLTP_PLM_M	maize	palmitate	M	1mzm	8006/8494	6/5
mLTP_CPR_B	maize	caprate	B	1fk0 with ligand inverted	8837/8482	6/5
mLTP_CPR_M	maize	caprate	M	1fk0	8837/8482	6/5

[a]The simulation name used, the LTP residue sequence, the ligand and binding mode, the starting structure for the simulation, the number of SPC water molecules in the rectangular periodic simulation box, and the number of chloride ions included are indicated. In columns 6 and 7, the number of water and chloride ions in the simulation with the protonated ligand is given first followed by the number in the simulation with the deprotonated ligand. Further details are given in Materials and Methods.

X-ray structure of mLTP with palmitate, where the ligand carboxylate headgroup is exposed, located on the surface of the protein interacting with the side chain of Tyr 81[9,13] and the hydrophobic tail of the ligand is buried in the internal cavity. Mode B is seen in the nuclear magnetic resonance (NMR) structure of the bLTP–palmitate complex, where the ligand is completely enclosed within the internal cavity, its headgroup positioned at the opposite end of the cavity close to Leu 14, Val 17, and Ile 69.[11] Our simulations show that for bLTP and mLTP the different ligand binding preferences do not result from changes to a single key residue involved in hydrogen bonding or the formation of a salt bridge with the ligand. Instead, they come from a range of small sequence changes spread throughout the protein structure.

MATERIALS AND METHODS

The MD simulations were conducted using the GROMOS biomolecular simulation software[24−27] and the GROMOS 54A7 force field parameter set.[28] The simulations reported in this work are summarized in Table 1. The coordinates for the bLTP–palmitate, mLTP–palmitate, and mLTP–caprate complexes used to start the simulations were taken from PDB entries 1be2 (model 1 used from the NMR set of structures),[11] 1mzm,[9] and 1fk0,[13] respectively. In the bLTP_PLM_M, mLTP_PLM_B, and mLTP_CPR_B simulations, the orientation of the ligand in the LTP internal cavity in the PDB structure was inverted using VMD[29] prior to starting the simulation. For each system, an initial simulation was run for 20 ns with a protonated palmitate or caprate headgroup. At the end of the simulation, the ligand was deprotonated and a 10 ns simulation was run (continued to 20 ns for the mLTP_CPR_B simulation). This simulation strategy, including the simulation times used, was found to be a successful one for characterizing bLTP–palmitate binding modes in previous work where a range of different simulation approaches were compared.[30]

In all the simulations, the Asp and Glu side chains in the protein were unprotonated and the two histidine side chains in bLTP were singly protonated at Nδ1. In each case, the protein–ligand complex was solvated in a rectangular box and minimum image periodic boundary conditions were applied. The minimum solute-box wall distance was set between 1.2 and 1.4 nm to give the same number of simple point charge (SPC) water molecules[31] in the simulations of a given system with ligands in binding mode M and B orientations (Table 1). Chloride ions were added to achieve overall neutrality of the systems; the number of chloride ions used in each simulation is listed in Table 1.

For each simulation, an initial equilibration scheme comprising six 20 ps simulations at temperatures of 60, 120, 180, 240, 280, and 310 K was used. During the first 80 ps of this equilibration, the solute atoms were restrained to their positions in the starting structure. Following equilibration, the simulations were continued at 310 K. All simulations were performed at a constant pressure of 1 atm, the temperature and pressure being maintained using the weak coupling algorithm,[32] with relaxation times of 0.1 ps (τ_T) and 0.5 ps (τ_p) and an isothermal compressibility of 4.575×10^{-4} (kJ mol^{-1} nm^{-3})$^{-1}$. The protein and solvent were separately coupled to the heat bath. The SHAKE algorithm[33] was used to constrain bond lengths and the geometry of the water molecules, with a relative geometric tolerance of 10^{-4} allowing for an integration time step of 2 fs. The center of mass motion was removed every 1000 time steps. Nonbonded interactions were calculated using a triple range cutoff scheme with cutoff radii of 0.8 and 1.4 nm. Interactions within 0.8 nm were evaluated every time step, and intermediate range interactions were updated every fifth time step. To account for the influence of the dielectric medium outside the cutoff sphere, a reaction-field force[34] with a relative dielectric permittivity (ε) of 61 was used.[35]

Analysis was performed with the GROMOS++ suite of analysis programs,[24] using coordinate and energy trajectories written to disk every 5 ps. The atom-positional root-mean-square deviation (rmsd) between the indicated atoms of two structures was calculated after the superposition of the heavy atoms of the protein backbone. The rmsd values for the ligand therefore reflect both changes in the ligand position within the LTP cavity and changes in its conformation. Regions of secondary structure were identified using the rules defined by Kabsch and Sander in DSSP.[36] The solvent accessible surface areas were calculated using the algorithm of Lee and Richards.[37] Hydrogen bonds were identified according to a geometric criterion: a hydrogen bond was assumed to exist if the hydrogen–acceptor distance was <0.25 nm and the donor–hydrogen–acceptor angle was >135°. To identify salt bridges, the hydrogen–acceptor distance was increased to 0.4 nm with no restriction on the donor–hydrogen–acceptor angle.[38] However, in the analysis of the mLTP_PLM_B and mLTP_CPR_B simulations, the distance cutoff was increased to 0.6 nm to assess the possibilities of short-lived salt bridge interactions mediated by water molecules between the ligands and Arg 19. The size and shape of the LTP internal cavity were determined using CASTp (Computed Atlas of Surface Topography of Proteins).[39]

RESULTS AND DISCUSSION

MD simulations were run for mLTP with either a palmitate or caprate ligand in the protein internal cavity in either the mode B or mode M orientation [simulations mLTP_PLM_B,

dx.doi.org/10.1021/bi4006573 | Biochemistry 2013, 52, 5029−5038

mLTP_PLM_M, mLTP_CPR_B, and mLTP_CPR_M (Table 1)] and for bLTP with a palmitate ligand in the protein internal cavity in either the mode B or mode M orientation (simulations bLTP_PLM_B and bLTP_PLM_M). In each of the simulations, the ligand carboxylate headgroup was protonated for the first 20 ns of the simulation. The ligand headgroup was then deprotonated and the simulation run for an additional 10 ns. The aim of protonating the headgroup for the first 20 ns is to keep the ligand in the LTP internal cavity for a sufficient amount of time that any suitable hydrogen bonding interactions have a chance to form. This approach was found to be successful in identifying the palmitate binding modes in previous simulations of bLTP.[30] Effectively, protonating the ligand headgroup weakens its highly favorable electrostatic interactions with SPC water, thus preventing rapid expulsion of the ligand from the protein cavity into the bulk solvent.

Figure 3 shows the variation in the atom-positional root-mean-square deviation (rmsd) of the ligand atoms from the starting structure and the ligand solvent accessible surface area (SASA) through the simulations. All three simulations with the ligand in the mode M orientation show similar behavior. The protonated ligands stay almost completely buried during the initial 20 ns of the simulations with a ligand rmsd of approximately 0.2 nm from the starting structure. When the ligands are deprotonated, there is a small increase in the ligand SASA to approximately 0.25 nm^2 and an increase in the ligand rmsd to approximately 0.35 nm, although for the mLTP_CPR_M simulation the ligand rmsd increases further in the last 5 ns of the simulation (see discussion later).

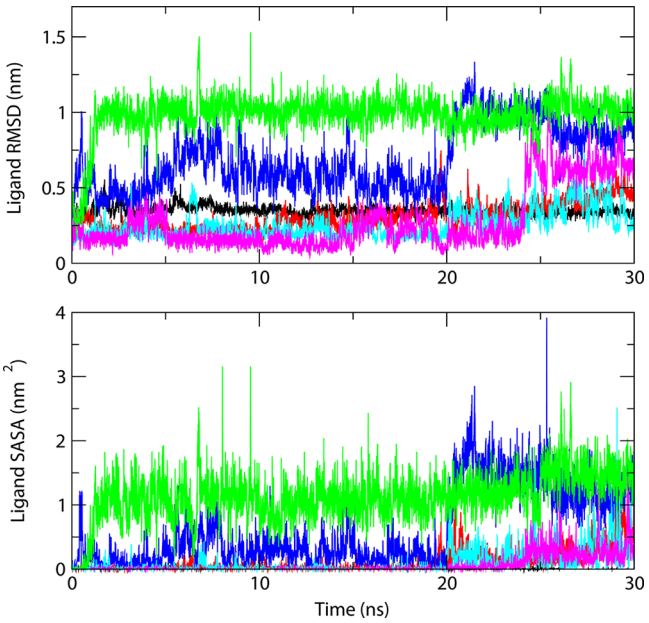

Figure 3. Time series showing variations in the atom-positional rmsd of the palmitate or caprate ligand atoms from the simulation starting structure (top) and the ligand solvent accessible surface area (bottom) through the simulations. The data for the different simulations are shown in the following colors: black for bLTP_PLM_B, red for bLTP_PLM_M, blue for mLTP_PLM_B, cyan for mLTP_PLM_M, green for mLTP_CPR_B, and magenta for mLTP_CPR_M. The data for the simulations with protonated ligands cover the period of 0−20 ns and those for the following simulations with unprotonated ligands the period of 20−30 ns. Note that in the calculation of the rmsd values the protein backbone (N, CA, and C) atoms were superimposed and the ligand rmsd was then calculated. These values therefore reflect changes in both the ligand conformation and its position in the LTP cavity.

The bLTP_PLM_B simulation shows ligand atom-positional rmsd and ligand SASA values of approximately 0.35 nm and 0 nm^2, respectively, throughout the simulation, with the ligand staying completely buried within the cavity. In contrast, the mLTP_PLM_B and mLTP_CPR_B simulations show large increases in ligand atom-positional rmsd and ligand SASA, with values of approximately 1.0 nm and 1.35 nm^2, respectively, by the end of the simulations. In these simulations, no persistent binding mode was found for the ligands within the mLTP cavity. By the end of the simulations, the ligand has moved significantly; its carbon chain remains in the cavity, but the ligand headgroup has come out of the cavity and is highly solvent exposed.

To assess energetically the ligand binding modes in the LTP cavities, the protein and ligand interaction energies were compared from 20 to 30 ns in the simulations when the ligands were unprotonated (Table 2). Note that this comparison does not take into account entropy. The three simulations with the ligand in the mode M orientation show similar favorable protein−ligand, ligand−ligand, and ligand−water noncovalent interaction energies, although for the bLTP_PLM_M and mLTP_PLM_M simulations the protein−ligand van der Waals energies (−152 and −159 kJ mol^{-1}, respectively) are more favorable than in the mLTP_CPR_M simulation (−101 kJ mol^{-1}). This difference reflects, at least in part, the different lengths of the carbon chains in the palmitate and caprate ligands (16 carbon atoms in palmitate vs 10 carbon atoms in caprate). Interestingly, the mLTP_CPR_M simulation shows a more favorable protein−ligand electrostatic energy (−212 kJ mol^{-1} for the mLTP_CPR_M simulation compared to −163 and −164 kJ mol^{-1} for the bLTP_PLM_M and mLTP_PLM_M simulations, respectively), which results in the total protein−ligand noncovalent energy terms overall being closely similar in the three binding mode M simulations.

The bLTP_PLM_B simulation has a significantly more favorable protein−ligand electrostatic energy (−390 kJ mol^{-1}) than the three simulations with the ligand in the mode M orientation. However, the ligand−water electrostatic energy is lower (−116 kJ mol^{-1}), reflecting the fact that the ligand retains a very low solvent accessibility even when deprotonated. This contrasts with the mLTP_PLM_B and mLTP_CPR_B simulations in which the ligand headgroup leaves the cavity and there are large negative ligand−water electrostatic energies (−559 and −540 kJ mol^{-1}, respectively) and small protein−ligand electrostatic energies (−10 and −28 kJ mol^{-1}, respectively).

Experimental studies of LTP−ligand complexes have demonstrated that the protein internal cavity has a structural plasticity; the cavity adapts its size and shape to accommodate the binding of different ligands.[10,13−16,40] Analysis of the LTP cavity in the simulations shows that this flexibility also enables the protein cavity to adjust to fluctuations in the position and conformation of a given ligand over time. Although the fluctuations in the cavity size and shape throughout the simulations make detailed analysis difficult, in general smaller cavity volumes are seen when the ligand is adopting binding mode B compared to binding mode M. For example, in the simulations of bLTP and mLTP with palmitate, the cavity volumes present at the end of the simulations are 0.69, 0.82, 0.57, and 0.84 nm^3 for the bLTP_PLM_B, bLTP_PLM_M,

dx.doi.org/10.1021/bi4006573 | Biochemistry 2013, 52, 5029−5038

Table 2. Contributions of the Covalent and Noncovalent Terms to the Potential Energies of the MD Simulations of Barley and Maize LTP with Unprotonated Palmitate and Caprate Ligands[a]

	energy (kJ mol^{-1}) (rmsd)					
	bLTP_PLM_B	bLTP_PLM_M	mLTP_PLM_B	mLTP_PLM_M	mLTP_CPR_B	mLTP_CPR_M
			Covalent			
protein	3025 (84)	3022 (81)	2748 (80)	2757 (83)	2743 (78)	2784 (83)
ligand	41 (10)	40 (10)	42 (10)	41 (10)	26 (8)	26 (8)
			Total Noncovalent			
protein−protein	−7373 (191)	−7639 (262)	−6260 (158)	−6265 (149)	−6250 (136)	−5973 (143)
protein−ligand	−553 (55)	−315 (80)	−145 (27)	−324 (78)	−106 (42)	−311 (55)
protein−water	−8877 (352)	−8589 (504)	−6829 (307)	−6654 (285)	−6889 (275)	−7205 (301)
ligand−ligand	−18 (3)	−18 (3)	−18 (3)	−18 (4)	−11 (3)	−11 (2)
ligand−water	−118 (41)	−364 (86)	−551 (45)	−349 (83)	−530 (55)	−308 (62)
			van der Waals			
protein−ligand	−164 (14)	−152 (12)	−135 (12)	−159 (11)	−78 (11)	−101 (10)
ligand−water	−3 (4)	−8 (11)	8 (13)	11 (11)	10 (14)	16 (11)
			Electrostatic			
protein−ligand	−390 (57)	−163 (83)	−10 (26)	−164 (77)	−28 (45)	−212 (55)
ligand−water	−116 (43)	−372 (91)	−559 (47)	−361 (84)	−540 (58)	−324 (64)

[a]In each case, the mean value is given, averaged over the trajectory, with the root-mean-square deviation in parentheses.

Table 3. Contributions of Individual Groups to the Nonbonded Protein−Ligand Electrostatic Energies (kJ mol^{-1}) in the MD Simulations of Barley and Maize LTP with Unprotonated Palmitate or Caprate Ligands[a]

protein atoms (barley/maize)	bLTP_PLM_B	bLTP_PLM_M	mLTP_ PLM_M	mLTP_CPR_M
Thr 15/Ser 16 (all atoms)	−105			
Tyr 16/Tyr 17 (backbone NH)	−53			
Val 17/Ala 18 (backbone NH)	−43			
Ser 24/Ser 26 (all atoms)	−65			
His 35/Asn 37 (side chain)		4	−2	−74
Arg 44/Arg 46 (side chain)		−126	−156	−155
Tyr 79/Tyr 81 (backbone NH)			−35	−2
Tyr 79/Tyr 81 (side chain)		−43	−5	−1
Ser 82/Ser 84 (backbone NH)		−28		

[a]In each case, the interaction involves the protein atoms listed with the carboxylate headgroup of the ligand. Data from the simulations of maize LTP with palmitate or caprate binding in mode B were omitted as the ligand headgroup leaves the LTP cavity in these simulations. Time series showing the fluctuations in these energies during the simulations are given in the Supporting Information.

mLTP_PLM_B, and mLTP_PLM_M simulations, respectively.

Binding Mode M. The simulations suggest that ligand binding mode M could be favorable in all three systems, i.e., for mLTP with either a palmitate or caprate ligand and for bLTP with a palmitate ligand. This is the binding mode that is seen experimentally for mLTP with palmitate. Table 3 compares contributions made by individual groups to the protein−ligand electrostatic energy in the simulations with unprotonated ligands. In all three simulations with binding mode M, the major contribution comes from the interaction of a conserved arginine side chain (Arg 44 in bLTP and Arg 46 in mLTP) with the ligand carboxylate headgroup (Table 3 and Figure 2C,E). This salt bridge has a population of 33−38% in the simulations (Table 4). Significant energetic contributions also come from interactions of the ligand carboxylate headgroup with the side chain of Tyr 79 and the NH group of Ser 82 in the bLTP_PLM_M simulation, with the NH group of Tyr 81 in the mLTP_PLM_M simulation, and with the side chain of Asn 37 in the mLTP_CPR_M simulation (Figure 2G). All of these groups form protein−ligand hydrogen bonds for a significant proportion of the simulations (Table 4). Although the ligand binding mode is similar in all three simulations, it is interesting that there are differences in which protein−ligand hydrogen bonds form. There are also changes in which hydrogen bonds are populated through the simulations. In addition, the ligand headgroups form many transient hydrogen bonds to different water molecules through the simulations (1543, 2235, and 1705 ligand−water hydrogen bonds in the 10 ns bLTP_PLM_M, mLTP_PLM_M, and mLTP_CPR_M simulations with an unprotonated ligand, respectively; all these hydrogen bonds have a population of <5%). Overall, the environment surrounding the ligand headgroup is quite dynamic. For example, the distance between the carboxylate carbon atom of the palmitate headgroup and the NH group of Tyr 81 in the mLTP_PLM_M simulation varies from 0.33 to 1.27 nm. Similarly, the distances between the carboxylate carbon atom of the palmitate headgroup and the side chain ND2 atom of Asn 37 in the mLTP_PLM_M and mLTP_CPR_M simulations range from 0.29 to 1.24 nm and from 0.29 to 1.13 nm, respectively (data for the mLTP_CPR_M simulation are shown in Figure 4). The fluctuations in the distances to the groups that form electrostatic interactions with the carboxylate headgroup lead to variations in the relative contributions to the protein−ligand electrostatic energy. Time series of energy contributions listed in Table 3 are given in the Supporting Information.

dx.doi.org/10.1021/bi4006573 | Biochemistry 2013, 52, 5029−5038

Table 4. Protein−Ligand Hydrogen Bonds and Salt Bridges with Populations of >10% in the Simulations of the Complexes of Barley and Maize LTP with Palmitate and Caprate Ligands[a]

protein atoms in hydrogen bond			barley mode B		barley mode M		maize mode M		maize mode M	
barley	maize	ligand atom	PLH	PLM	PLH	PLM	PLH	PLM	CPH	CPR
Thr 15 NH		O1		50						
Thr 15 NH		O2		45						
Thr 15 OH		O2		54						
Tyr 16 NH		O1		36						
Tyr 16 NH		O2	19	66						
Val 17 NH		O1		80						
Val 17 NH		O2	45							
Ser 24 NH		O1	25							
Ser 24 NH		O2	16	93						
	Asn 37 ND2	O2					45		60	33
	Asn 37 ND2	O1								41
Arg 44 NEH	Arg 46 NEH	O1				10				
Arg 44 NEH	Arg 46 NEH	O2								
Arg 44 NH2		O2			14					
	Tyr 81 NH	O2					23	24		
	Tyr 81 NH	O1						41		
Tyr 79 OH	Tyr 81 OH	O1				38			99	
Tyr 79 OH		O2				34				
Ser 82 NH		O1				18				
Ser 82 NH		O2				32				
Tyr 91 O1	Asn 93 O1	O1H			18		14			
Tyr 91 O2	Asn 93 O2	O1H			11		15			
salt bridge										
Arg 44 side chain	Arg 46 side chain	headgroup				37		33		38

[a]PLH indicates the 20 ns simulations with protonated palmitate, PLM the continuation simulations with deprotonated palmitate, CPH the 20 ns simulation with protonated caprate, and CPR the continuation simulation with deprotonated caprate. Note that the simulations of maize LTP with palmitate and with caprate in mode B were omitted as there were no protein−ligand hydrogen bonds or salt bridges with populations of >10%.

Binding Mode B. The bLTP_PLM_B simulation is the only simulation with the ligand in binding mode B that shows persistent ligand binding within the LTP cavity. This is the binding mode that is observed experimentally for bLTP with palmitate. Table 3 shows that in this simulation there are significant contributions to the protein−ligand electrostatic energy from the backbone NH groups of Thr 15, Tyr 16, Val 17, and Ser 24 and from the side chains of Thr 15. All these groups form protein−ligand hydrogen bonds in the simulation with populations of 36−93% (Table 4). As has been identified previously,[30] the formation of protein−ligand hydrogen bonds in the bLTP−palmitate complex appears to exploit the irregular intraprotein hydrogen bonding pattern seen in helix A (residues 4−19), which is caused by the presence of a proline at residue 12. Experimental NMR hydrogen exchange studies of bLTP identified slow amide proton exchange rates for residues 6, 9−11, 13, 14, 17, and 18 in helix A of the protein.[41] On the basis of these data, NH(i)−CO(i−4) hydrogen bond restraints had been included for the NH groups of residues 9−11 and 17−19 and an NH(i)−CO(i−3) hydrogen bond restraint for the NH group of residue 13 in the NMR structure determination of the bLTP−palmitate complex.[11] However, residues 14−16 are not involved in helical hydrogen bonds in this NMR structure. In the bLTP_PLM_B simulation, the hydrogen bonding pattern in the center of helix A is quite dynamic with the NH groups of residues 13 and 14 forming NH(i)−CO(i−4) hydrogen bonds with populations of 19 and 46%, respectively, while helical hydrogen bonds for residues 15−17 are virtually absent (≤1%). The absence of these helical hydrogen bonds means that the NH groups of residues 15−17 are available for hydrogen bonding to palmitate (Table 4).

It is likely that the fluctuating helical hydrogen bonding pattern in the center of helix A allows the bLTP−palmitate binding mode to be quite dynamic with other backbone NH groups in helix A being involved in hydrogen bonding to palmitate over time.[30] In addition, a number of water molecules form short-lived hydrogen bonds with the palmitate headgroup in the LTP cavity during the simulation. In particular, 65 different ligand−water hydrogen bonds are observed through the 10 ns simulation with unprotonated palmitate. One of these is populated for 10% of the simulation, while the others are populated <3% of the time. The number of transient ligand−water hydrogen bonds is much smaller than the number seen in the mode M simulations (1543−2235 ligand−water hydrogen bonds), presumably reflecting the fact that the ligand headgroup is positioned in the interior of the cavity.

mLTP also contains a proline in the center of helix A (Pro 13), and the mLTP simulations show disrupted hydrogen bonding patterns in helix A with helical hydrogen bonds for residues 16 and 17 having populations of ≤5%. Thus, the NH groups of these residues in helix A would be available for hydrogen bonding to the ligand in the mLTP_PLM_B and mLTP_CPR_B simulations. However, protein−ligand hydrogen bonds from backbone NH groups in helix A are not seen in the simulations of mLTP with palmitate or caprate in the mode B orientation. One reason for this may be the difference in sequence between mLTP and bLTP in the loop region between helices A and B (residues 20−24 in bLTP and residues 21−26 in mLTP). In particular, in mLTP, there is an insertion of a

dx.doi.org/10.1021/bi4006573 | Biochemistry 2013, 52, 5029−5038

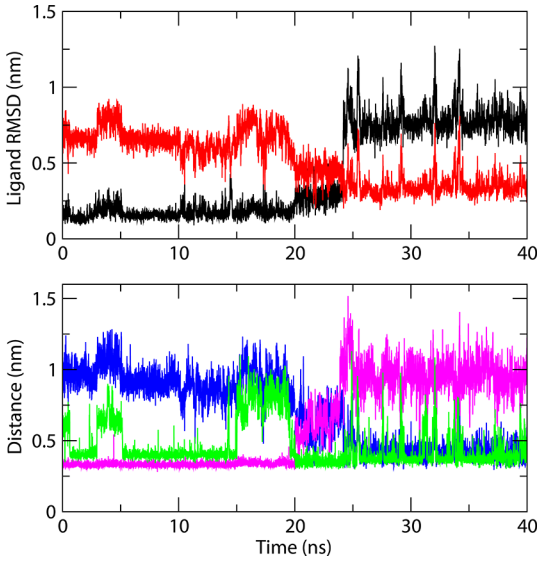

Figure 4. Time series (top) showing variations in the atom-positional rmsd of the caprate ligand atoms during the mLTP_CPR_M simulation. The rmsd values of residues C1−C10 in caprate with respect to residues C7−C16 and C1−C10 of palmitate in the PDB entry 1mzm crystal structure[9] are colored black and red, respectively. For the rmsd calculations, the protein backbone (N, CA, and C) atoms were superimposed and the ligand rmsd was then calculated. Time series (bottom) showing variations in the distances between caprate C1 and Arg 46 NE (blue), caprate C1 and Tyr 81 OH (magenta), and caprate C1 and Asn 37 ND2 (green) through the mLTP_CPR_M simulation. In each case, the data for the simulation with protonated caprate are plotted from 0 to 20 ns and those for the following simulation with unprotonated caprate from 20 to 40 ns.

glutamine residue at position 21 and a sequence change of Pro 21 in bLTP to a serine residue (Ser 23) in mLTP (Figure 1) that gives this loop region quite a different orientation in the two proteins. In the bLTP_PLM_B simulation, Ser 24 is close to the palmitate headgroup (mean Ser 24 N−palmitate O1 distance of 0.49 nm). The positioning of Ser 24 close to residues 15−17 in helix A means that the ligand headgroup is in an environment where it is surrounded by hydrogen bond donors (Figure 2B). In the mLTP_PLM_B simulation, in contrast, even in the initial 20 ns during which the protonated ligand headgroup remains in the LTP cavity, the mean distance from the Ser 26 N atom to the palmitate O1 headgroup atom is 1.48 nm and the same cluster of hydrogen bond donor groups is unavailable for binding to the palmitate headgroup.

The difference in the AB loop region between bLTP and mLTP and consequent changes to the environment surrounding the binding site of the ligand headgroup in orientation B may explain, at least in part, the different binding modes observed experimentally for bLTP and mLTP with palmitate. To understand in more detail the difference in ligand binding preferences, the first 20 ns of the mLTP_PLM_B, mLTP_CPR_B, and bLTP_PLM_B simulations have been compared. In this part of the simulations, the ligand headgroups are protonated and are positioned, at least initially, in a similar place within the cavity. Here, compared to the simulations with the unprotonated ligand, the electrostatic energy terms involving the ligand are smaller (protein−ligand electrostatic energies range from −2 to −33 kJ mol^{-1} and ligand−water electrostatic energies from −50 to −89 kJ mol^{-1} in the three simulations). The largest noncovalent energy terms involving the ligand for the palmitate simulations are the protein−ligand van der Waals energies (mLTP_PLM_B, −169 kJ mol^{-1}; mLTP_CPR_B, −84 kJ mol^{-1}; bLTP_PLM_B, −186 kJ mol^{-1}).

The protein−ligand van der Waals energies are the sums of small contributions from many different atoms. Table 5 gives the contributions to this term from the residues with nonpolar side chains that line the LTP internal cavity (time series, showing the variations in these energies through the simulations, are available as Supporting Information). Caprate, which has a shorter carbon chain, has less favorable protein−ligand van der Waals contributions than palmitate, especially involving groups at the bottom of the cavity. Many of the residues that line the internal cavity in mLTP and bLTP are identical [Val 7 and Val 6, Cys 14 and Cys 13, Val 33 and Val 31, Leu 36 and Leu 34, Leu 53 and Leu 51, Ile 71 and Ile 69, Tyr 81 and Tyr 79, and Ile 83 and Ile 81 for mLTP and bLTP, respectively (Table 5)]. However, there are some sequence differences that contribute to differences in the protein−ligand van der Waals energy in the mLTP_PLM_B and bLTP_PLM_B simulations. In particular, in the bottom of the LTP cavity, His 35 and Val 47 in bLTP are changed to Asn 37 and Ala 49, respectively, in mLTP with a reduction in the protein−ligand van der Waals energy (−8 kJ mol^{-1} in bLTP compared to −3 kJ mol^{-1} in mLTP). In addition, in helix A, there is a persistent salt bridge involving the side chains of Asp 7 and Lys 11 in bLTP (57% population in the bLTP_PLM_B simulation). This salt bridge is missing in mLTP where the corresponding residues are both alanines (Figure 1). A higher population for the residue 11 NH−residue 7 CO helical hydrogen bond is seen during the first 20 ns of the bLTP_PLM_B simulation (93%) compared to the equivalent residue 12 NH−residue 8 CO hydrogen bond in the mLTP_PLM_B simulation (52%). This suggests that the Arg 7−Lys 11 salt bridge may be helping to maintain this helical turn in bLTP. This salt bridge is positioned on the protein exterior with Val 6 and Met 10 positioned on the other face of the helix lining the protein internal cavity. In the bLTP_PLM_B simulation, where the helical turn in this region is highly populated, these residues contribute very favorably to the protein−ligand van der Waals energy (−14 kJ mol^{-1}). In contrast, in mLTP where the helical turn fluctuates more, the contribution from the corresponding residues (Val 7 and Ile 11) is smaller (−7 kJ mol^{-1}).

There are also sequence differences between mLTP and bLTP for residues on the protein surface at the entrance to the internal cavity, close to where the headgroup moves in the mLTP_PLM_B and mLTP_CPR_B simulations. In particular, Arg 19 and Asn 55 in mLTP are changed to Gln 18 and Gly 53, respectively, in bLTP (Figure 1). Although no persistent hydrogen bonds are formed between the side chains of these residues and the ligand headgroup in the mLTP simulations, the more positive environment at the entrance to the cavity may help destabilize the B ligand binding mode in mLTP. Consistent with this, using a long cutoff distance criterion of 0.6 nm, a salt bridge between the Arg 19 side chain and the caprate headgroup with a population of 16% is seen in the mLTP_CPR_B simulation with unprotonated caprate. The population of this salt bridge in the corresponding mLTP_PLM_B simulation is only 5%.

Palmitate Binding. The different binding mode preference for palmitate with mLTP and bLTP observed experimentally appears to result from the combined effects of a number of

dx.doi.org/10.1021/bi4006573 | *Biochemistry* 2013, 52, 5029−5038

Table 5. Contributions to the Nonbonded Protein−Ligand van der Waals Energies (kJ mol^{-1}) in the MD Simulations of Barley and Maize LTP with Protonated Palmitate or Protonated Caprate Ligands Binding in the Mode B Orientation[a]

protein side chain atoms of LTP	ligand atoms	bLTP_PLM_B	mLTP_PLM_B	mLTP_CPR_B
top of cavity	noncharged carbons	−12	−12	−8
barley				
Cys 13, Leu 14, Ile 69				
maize				
Cys 14, Ile 15, Ile 71				
top of cavity	noncharged carbons	−14	−7	−5
barley				
Val 6, Met 10				
maize				
Val 7, Ile 11				
middle of cavity	noncharged carbons	−18	−20	−6
barley				
Val 31, Leu 51, Ile 81				
maize				
Val 33, Leu 53, Ile 83				
bottom of cavity	noncharged carbons	−8	−9	−1
barley				
Leu 34, Tyr 79				
maize				
Leu 36, Tyr 81				
bottom of cavity	noncharged carbons	−8	−3	0
barley				
His 35, Val 47				
maize				
Asn 37, Ala 49				
all protein atoms	noncharged carbons (per carbon atom)	−162 (−11)	−154 (−10)	−74 (−8)

[a]The data are the mean values over the 10−20 ns time window. Time series showing the fluctuations in these energies during the simulations are given in the Supporting Information.

sequence changes between the two proteins. The simulations suggest that both proteins could bind ligands in the mode M orientation. In this case, the dominant interaction would be a salt bridge between the charged carboxylate headgroup of the ligand and a conserved arginine side chain (Arg 44 in bLTP and Arg 46 in mLTP). The mLTP_PLM_M and bLTP_PLM_M simulations show very similar protein−ligand interaction energies, and this binding mode is experimentally seen for mLTP but not for bLTP. Sequence changes between bLTP and mLTP result in a significant difference for binding mode B where the protein−ligand interaction energy is particularly favorable in the bLTP_PLM_B simulation. Consequently, this binding orientation is preferred for bLTP, in agreement with the experimental NMR structure.[11] In this respect, it is interesting that Douliez et al.[40] have reported, on the basis of fluorescence and isothermal titration calorimetry data, that bLTP can bind two molecules of lyso-myristoyl-phosphatidylcholine and also of ω-hydroxypalmitic acid in the protein internal cavity. Dual ligand binding has also been seen in the structures of rice LTP with palmitate[15] and wheat LTP with lyso-myristoyl-phosphatidylcholine,[14] with the two ligands lying in head-to-tail manner. It is therefore likely that in bLTP when two ligand molecules are accommodated in the internal cavity, one will bind in mode B and the other will adopt the opposite orientation with its headgroup forming a salt bridge with Arg 44 in a manner similar to that seen in the bLTP_PLM_M simulation.

Caprate Binding. Han et al.[13] proposed that the caprate ligand may bind to mLTP in both the B and M orientations. This suggestion was based on the absence of the bifurcated shape of the carboxylate moiety in the electron density map from X-ray diffraction studies of the mLTP−caprate complex. No hydrogen bonds are defined between the carboxylate group of caprate and the protein in the X-ray structure.[13] As discussed above, no persistent binding mode for caprate is identified in the internal cavity in the mLTP_CPR_B simulation, but in the mLTP_CPR_M simulation, the ligand remains in the mLTP cavity and shows the most favorable protein−ligand electrostatic interaction energy of the three mode M simulations reported here.

An interesting feature of the mLTP_CPR_M simulation is an increase in the ligand atom-positional rmsd in the final 5 ns of the 30 ns simulation from approximately 0.2 to 0.7 nm. To characterize the changes occurring in this final 5 ns, the mLTP_CPR_M simulation was continued for a further 10 ns. No further significant increase in the ligand atom-positional rmsd was observed. Calculation of the atom-positional rmsd of the caprate ligand in the mLTP_CPR_M simulation with respect to the position of the palmitate ligand in the mLTP−palmitate crystal structure (PDB entry 1mzm[9]) shows that initially C1−C10 of caprate are positioned in the cavity in a manner similar to that of the carbon end of the palmitate ligand (C7−C16). However, around the 25 ns time point in the mLTP_CPR_M simulation, the ligand moves so it becomes positioned in a manner similar to that of the carboxylate end of the palmitate ligand (C1−C10) (Figures 2B and 4). Initially, the caprate headgroup makes a very persistent hydrogen bond to the side chain of Tyr 79. However, between 20 and 25 ns, the caprate carboxylate headgroup moves closer to the side

dx.doi.org/10.1021/bi4006573 | Biochemistry 2013, 52, 5029−5038

chain of Arg 46 (Figure 4). In both positions, hydrogen bonding to the side chain of Asn 37 is observed.

These changes observed in the simulation suggest that caprate may have quite a dynamic binding mode in the LTP cavity, with a variety of hydrogen bonds involving the key residues in the mode M binding site. Indeed, as discussed earlier, a feature of the mode M binding seems to be the proximity of a number of hydrogen bond donors with differences being seen between the protein−ligand hydrogen bonds in the bLTP_PLM_M, mLTP_PLM_M, and mLTP_CPR_M simulations. The dynamic nature of the binding mode for caprate proposed on the basis of the simulation results would explain the absence of clear electron density for the carboxylate headgroup in the X-ray structure determination. No persistent ligand binding was found for caprate in the mLTP_CPR_B simulation, which suggests that the initial proposal of population of both mode B and mode M ligand binding orientations is unlikely.

CONCLUSIONS

The MD simulations reported here complement a computational study of binding of ligands to a range of plant LTPs reported by Pacios et al.[7] This study considered complexes of maize, wheat, barley, rice, and peach LTP with a range of ligands bound in the two orientations, B and M, considered here. Using X-ray, NMR, and model structures optimized with short MD simulations (in general 100 ps, although longer 4 ns simulations were run for two complexes of peach and wheat LTP), electrostatic potentials, solvation energies, properties of the protein−ligand interfaces, and estimates of binding free energies were calculated for the different complexes. Some correlations were seen between differences in the electrostatic potential on the protein surface in the different species of LTP and their preferences for ligand binding orientation. However, no differences in binding free energies were seen between the two ligand binding modes.[7]

The results reported here show that the X-ray and NMR structures for the bLTP and mLTP complexes do not provide a complete picture of ligand binding in the internal cavity. Long MD simulations starting from these structures, using both protonated and unprotonated ligands, are needed to establish the details of the ligand binding behavior, which involves fluctuating combinations of hydrogen bonds, salt bridges, and many different nonpolar contacts. With the 30 ns MD simulations reported here, a good correlation has been seen between the ligand binding modes observed experimentally for maize and barley LTP with palmitate and the preferred binding modes identified in the simulations. Detailed analyses of the simulations have shown that the different ligand binding modes seen in the two systems result at least in part from differences in the sequences and structural preferences of the protein in the AB loop region and in the helix A region together with changes in the nature of the residues lining the base of the hydrophobic cavity and the protein surface. In addition, from the MD simulations of mLTP with caprate, we have been able to propose that binding mode M is preferred in this system rather than the originally suggested mixture of binding modes M and B. However, with the shorter carbon chain of caprate, the ligand exhibited more mobility within the mLTP cavity than was seen with the palmitate ligands. This is likely to have given rise to the absence of electron density for the ligand headgroup in the X-ray structure determination.[13]

ASSOCIATED CONTENT

Supporting Information

Time series showing the variations in the contributions made by individual groups to the nonbonded protein−ligand electrostatic energy or protein−ligand van der Waals energy during the simulations. The mean values from these time series are listed in Tables 3 and 5. This material is available free of charge via the Internet at http://pubs.acs.org.

AUTHOR INFORMATION

Corresponding Author

*Department of Chemistry, University of Oxford, Inorganic Chemistry Laboratory, South Parks Road, Oxford OX1 3QR, U.K. E-mail: lorna.smith@chem.ox.ac.uk. Phone: +44 1865 272694. Fax: +44 1865 272690.

Present Address

§J.R.A.: Centre for Theoretical Chemistry and Physics, Institute of Natural and Mathematical Sciences, Massey University, Albany, Private Bag 102904, North Shore City, 0745 Auckland, New Zealand.

Funding

W.F.v.G. thanks the Swiss National Science Foundation (Grant 200020-137827) and its National Competence Center for Research (NCCR) in Structural Biology and the European Research Council (Grant 228076) for financial support. L.J.S. thanks the ETH for financial support during her visit as a Guest Professor.

Notes

The authors declare no competing financial interest.

ACKNOWLEDGMENTS

L.J.S. acknowledges the use of the Oxford Supercomputing Centre (OSC) in conducting out some of this work.

ABBREVIATIONS

LTP, nonspecific lipid transfer protein 1; bLTP, barley nonspecific lipid transfer protein 1; mLTP, maize nonspecific lipid transfer protein 1; MD, molecular dynamics; PDB, Protein Data Bank; rmsd, root-mean-square deviation; SASA, solvent accessible surface area; SPC, simple point charge.

REFERENCES

(1) Kader, J. C. (1996) Lipid-transfer proteins in plants. *Annu. Rev. Plant Physiol. Plant Mol. Biol. 47*, 627−654.

(2) Douliez, J. P., Michon, T., Elmorjani, K., and Marion, D. (2000) Structure, biological and technological functions of lipid transfer proteins and indolines, the major lipid binding proteins from cereal kernels. *J. Cereal Sci. 32*, 1−20.

(3) Salcedo, G., Sanchez-Monge, R., Barber, D., and Diaz-Perales, A. (2007) Plant non-specific lipid transfer proteins: An interface between plant defence and human allergy. *Biochim. Biophys. Acta 1771*, 781−791.

(4) Garcia-Olmedo, F., Molina, A., Segura, A., and Moreno, M. (1995) The defensive role of nonspecific lipid-transfer proteins in plants. *Trends Microbiol. 3*, 72−74.

(5) Kader, J. C. (1997) Lipid-transfer proteins: A puzzling family of plant proteins. *Trends Plant Sci. 2*, 66−70.

(6) Yeats, T. H., and Rose, J. K. C. (2008) The biochemistry and biology of extracellular plant lipid-transfer proteins (LTPs). *Protein Sci. 17*, 191−198.

(7) Pacios, L. F., Gomez-Casado, C., Tordesillas, L., Palacin, A., Sanchez-Monge, R., and Diaz-Perales, A. (2012) Computational study of ligand binding in lipid transfer proteins: Structures, interfaces, and

free energies of protein-lipid complexes. *J. Comput. Chem. 33*, 1831−1844.
(8) Boutrot, F., Guirao, A., Alary, R., Joudrier, P., and Gautier, M. F. (2005) Wheat non-specific lipid transfer protein genes display a complex pattern of expression in developing seeds. *Biochim. Biophys. Acta 1730*, 114−125.
(9) Shin, D. H., Lee, J. Y., Hwang, K. Y., Kim, K. K., and Suh, S. W. (1995) High resolution crystal structure of the nonspecific lipid transfer protein from maize seedlings. *Structure 3*, 189−199.
(10) Lerche, M. H., Kragelund, B. B., Bech, L. M., and Poulsen, F. M. (1997) Barley lipid-transfer protein complexed with palmitoyl CoA: The structure reveals a hydrophobic binding site that can expand to fit both large and small lipid-like ligands. *Structure 5*, 291−306.
(11) Lerche, M. H., and Poulsen, F. H. (1998) Solution structure of barley lipid transfer protein complexed with palmitate. Two different binding modes of palmitate in the homologous maize and barley nonspecific lipid transfer proteins. *Protein Sci. 7*, 2490−2498.
(12) Sodano, P., Caille, A., Sy, D., dePerson, G., Marion, D., and Ptak, M. (1997) H-1 NMR and fluorescence studies of the complexation of DMPG by wheat non-specific lipid transfer protein. Global fold of the complex. *FEBS Lett. 416*, 130−134.
(13) Han, G. W., Lee, J. Y., Song, H. K., Chang, C. S., Min, K., Moon, J., Shin, D. H., Kopka, M. L., Sawaya, M. R., Yuan, H. S., Kim, T. D., Choe, J., Lim, D., Moon, H. J., and Suh, S. W. (2001) Structural basis of non-specific lipid binding in maize lipid-transfer protein complexes revealed by high-resolution X-ray crystallography. *J. Mol. Biol. 308*, 263−278.
(14) Charvolin, D., Douliez, J. P., Marion, D., Cohen-Addad, C., and Pebay-Peyroula, E. (1999) The crystal structure of a wheat nonspecific lipid transfer protein (ns-LTP1) complexed with two molecules of phospholipid at 2.1 Å resolution. *Eur. J. Biochem. 264*, 562−568.
(15) Cheng, H. C., Cheng, P. T., Peng, P. Y., Lyu, P. C., and Sun, Y. J. (2004) Lipid binding in rice nonspecific lipid transfer protein-1 complexes from *Oryza sativa*. *Protein Sci. 13*, 2304−2315.
(16) Tassin-Moindrot, S., Caille, A., Douliez, J. P., Marion, D., and Vovelle, F. (2000) The wide binding properties of a wheat nonspecific lipid transfer protein: Solution structure of a complex with prostaglandin B-2. *Eur. J. Biochem. 267*, 1117−1124.
(17) Pasquato, N., Berni, R., Folli, C., Folloni, S., Cianci, M., Pantano, S., Helliwell, J. R., and Zanotti, G. (2006) Crystal structure of peach Pru p 3, the prototypic member of the family of plant non-specific lipid transfer protein pan-allergens. *J. Mol. Biol. 356*, 684−694.
(18) Chothia, C., and Lesk, A. M. (1986) The relation between the divergence of sequence and structure in proteins. *EMBO J. 5*, 823−826.
(19) Bartlett, G. J., Borkakoti, N., and Thornton, J. M. (2003) Catalysing new reactions during evolution: Economy of residues and mechanism. *J. Mol. Biol. 331*, 829−860.
(20) Eyre-Walker, A., and Keightley, P. D. (2007) The distribution of fitness effects of new mutations. *Nat. Rev. Genet. 8*, 610−618.
(21) Soskine, M., and Tawfik, D. S. (2010) Mutational effects and the evolution of new protein functions. *Nat. Rev. Genet. 11*, 572−582.
(22) Studer, R. A., Dessailly, B. H., and Orengo, C. A. (2013) Residue mutations and their impact on protein structure and function: Detecting beneficial and pathogenic changes. *Biochem. J. 449*, 581−594.
(23) Needleman, S. B., and Wunsch, C. D. (1970) A general method applicable to search for similarities in amino acid sequence of two proteins. *J. Mol. Biol. 48*, 443−453.
(24) Eichenberger, A. P., Allison, J. R., Dolenc, J., Geerke, D. P., Horta, B. A. C., Meier, K., Oostenbrink, C., Schmid, N., Steiner, D., Wang, D., and van Gunsteren, W. F. (2011) GROMOS++ Software for the analysis of biomolecular simulation trajectories. *J. Chem. Theory Comput. 7*, 3379−3390.
(25) Schmid, N., Christ, C. D., Christen, M., Eichenberger, A. P., and van Gunsteren, W. F. (2012) Architecture, implementation and parallelisation of the GROMOS software for biomolecular simulation. *Comput. Phys. Commun. 183*, 890−903.
(26) Schmid, N., Allison, J. R., Dolenc, J., Eichenberger, A. P., Kunz, A.-P. E., and van Gunsteren, W. F. (2011) Biomolecular structure refinement using the GROMOS simulation software. *J. Biomol. NMR 51*, 265−281.
(27) http://www.gromos.net.
(28) Schmid, N., Eichenberger, A. P., Choutko, A., Riniker, S., Winger, M., Mark, A. E., and van Gunsteren, W. F. (2011) Definition and testing of the GROMOS force-field versions 54A7 and 54B7. *Eur. Biophys. J. 40*, 843−856.
(29) Humphrey, W., Dalke, A., and Schulten, K. (1996) VMD: Visual Molecular Dynamics. *J. Mol. Graphics 14*, 33−38.
(30) Smith, L. J., van Gunsteren, W. F., and Allison, J. R. (2013) Multiple binding modes for palmitate to barley lipid transfer protein facilitated by the presence of proline 12. *Protein Sci. 22*, 56−64.
(31) Berendsen, H. J. C., Postma, J. P. M., van Gunsteren, W. F., and Hermans, J. (1981) Interaction models for water in relation to protein hydration. In *Intermolecular Forces* (Pullman, B., Ed.) pp 331−342, Reidel, Dordrecht, The Netherlands.
(32) Berendsen, H. J. C., Postma, J. P. M., van Gunsteren, W. F., Dinola, A., and Haak, J. R. (1984) Molecular dynamics with coupling to an external bath. *J. Chem. Phys. 81*, 3684−3690.
(33) Ryckaert, J. P., Ciccotti, G., and Berendsen, H. J. C. (1977) Numerical integration of cartesian equations of motion of a system with constraints: Molecular dynamics of n-alkanes. *J. Comput. Phys. 23*, 327−341.
(34) Tironi, I. G., Sperb, R., Smith, P. E., and van Gunsteren, W. F. (1995) A generalised reaction field method for molecular dynamics simulations. *J. Chem. Phys. 102*, 5451−5459.
(35) Heinz, T. N., van Gunsteren, W. F., and Hunenberger, P. H. (2001) Comparison of four methods to compute the dielectric permittivity of liquids from molecular dynamics simulations. *J. Chem. Phys. 115*, 1125−1136.
(36) Kabsch, W., and Sander, C. (1983) Dictionary of protein secondary structure: Pattern recognition of hydrogen bonded and geometical features. *Biopolymers 22*, 2577−2637.
(37) Lee, B., and Richards, F. M. (1971) Interpretation of protein structures: Estimation of static accessibility. *J. Mol. Biol. 55*, 379−400.
(38) Barlow, D. J., and Thornton, J. M. (1983) Ion-pairs in proteins. *J. Mol. Biol. 168*, 867−885.
(39) Dundas, J., Ouyang, Z., Tseng, J., Binkowski, A., Turpaz, Y., and Liang, J. (2006) CASTp: Computed atlas of surface topography of proteins with structural and topographical mapping of functionally annotated residues. *Nucleic Acids Res. 34*, W116−W118.
(40) Douliez, J. P., Jegou, S., Pato, C., Molle, D., Tran, V., and Marion, D. (2001) Binding of two mono-acylated lipid monomers by the barley lipid transfer protein, LTP1, as viewed by fluorescence, isothermal titration calorimetry and molecular modelling. *Eur. J. Biochem. 268*, 384−388.
(41) Heinemann, B., Andersen, K. V., Nielsen, P. R., Bech, L. M., and Poulsen, F. M. (1996) Structure in solution of a four-helix lipid binding protein. *Protein Sci. 5*, 13−23.
(42) Rice, P., Longden, I., and Bleasby, A. (2000) EMBOSS: The European Molecular Biology Open Software Suite. *Trends Genet. 16*, 276−277.